Ore Geology Reviews 75 (2016) 16–28

Contents lists available at ScienceDirect

Ore Geology Reviews

journal homepage: www.elsevier.com/locate/oregeorev

Mapping mineral prospectivity for Cu polymetallic mineralization in southwest Fujian Province, China

Yuan Gao [a], Zhenjie Zhang [b], Yihui Xiong [a], Renguang Zuo [a,*]

[a] State Key Laboratory of Geological Processes and Mineral Resources, China University of Geosciences, Wuhan 430074, China
[b] School of Earth Sciences and Resources, China University of Geosciences, Beijing 100083, China

ARTICLE INFO

Article history:
Received 30 August 2015
Received in revised form 1 December 2015
Accepted 8 December 2015
Available online 10 December 2015

Keywords:
Mineral prospectivity mapping
Porphyry–epithermal Cu
Fuzzy weights of evidence
Random forest
Prediction–area plot
Receiver operating characteristics

ABSTRACT

In this study, both the fuzzy weights of evidence (FWofE) and random forest (RF) methods were applied to map the mineral prospectivity for Cu polymetallic mineralization in southwestern Fujian Province, which is an important Cu polymetallic belt in China. Recent studies have revealed that the Zijinshan porphyry–epithermal Cu deposit is associated with Jurassic to Cretaceous (Yanshanian) intermediate to felsic intrusions and faulting tectonics. Evidence layers, which are key indicators of the formation of Zijinshan porphyry–epithermal Cu mineralization, include: (1) Jurassic to Cretaceous intermediate–felsic intrusions; (2) mineralization-related geochemical anomalies; (3) faults; and (4) Jurassic to Cretaceous volcanic rocks. These layers were determined using spatial analyses in support by GeoDAS and ArcGIS based on geological, geochemical, and geophysical data. The results demonstrated that most of the known Cu occurrences are in areas linked to high probability values. The target areas delineated by the FWofE occupy 10% of the study region and contain 60% of the total number of known Cu occurrences. In comparison with FWofE, the resulting RF areas occupy 15% of the study area, but contain 90% of the total number of known Cu occurrences. The normalized density value of 1.66 for RF is higher than the 1.15 value for FWofE, indicating that RF performs better than FWofE. Receiver operating characteristics (ROC) were used to validate the prospectivity model and check the effects of overfitting. The area under the ROC curve (AUC) was greater than 0.5, indicating that both prospectivity maps are useful in Cu polymetallic prospectivity mapping in southwestern Fujian Province.

1. Introduction

The origin of mineral prospectivity modeling (MPM) can be traced back to the works of mathematical geologists such as Harris (1965, 1969); Sinclair and Woodsworth (1970); Agterberg (1971, 1973, 1974), and Bonham-Carter (1994). Methods for GIS-based mineral prospectivity analysis and predictive modeling have been developed over the past 30 years. A number of mathematical methods and models have been introduced for MPM in an attempt to provide objective tools for the integration of multi-source data to narrow down target areas for ground exploration at different scales. The integration functions applied in MPM vary from simple arithmetic or logical operators to complex mathematical functions. These methods can be generally subdivided into knowledge- and data-driven categories, depending on whether the function's parameters are estimated heuristically using theoretical or empirically based knowledge on the statistical spatial relationships between known deposits of the targeted type and predictor maps. Knowledge-driven methods, such as fuzzy logic (An et al., 1991; Ford et al., 2015), Boolean logic (Bonham-Carter and Cox, 1995; Carranza et al., 1999), and evidential belief (An et al., 1994; Carranza et al., 2005; Carranza, 2009), use expert opinions to assign the weights for each evidence map. Data-driven approaches, such as weights of evidence (WofE: Bonham-Carter et al., 1990; Liu et al., 2014; Ford et al., 2015), Bayesian network classifiers (Porwal et al., 2006), neural networks (Singer and Kouda, 1996; Brown et al., 2000; Oh and Lee, 2010), and support vector machine (Zuo and Carranza, 2011; Geranian et al., 2015) are based on quantitative measures of spatial associations between known mineral occurrences and multiple prospecting datasets (Bonham-Carter, 1994; Carranza, 2011; Porwal and Carranza, 2015). Knowledge-driven approaches are commonly applied in greenfields, where no or very few mineral occurrences have been discovered. In contrast, data-driven mineral prospectivity models are suitable for "brownfields" (moderately or well-explored regions) where the goal is to define new exploration targets for mineral deposits of the desired type.

When using ordinary WofE, evidence maps should be converted into binary or ternary form so that maps of different types can be compared and integrated into a single index of favourability or probability (Agterberg, 1989; Agterberg et al., 1990; Bonham-Carter et al., 1990). Cheng and Agterberg (1999) proposed the fuzzy weights of evidence (FWofE) method, an extension of the ordinary WofE method, to

* Corresponding author.
E-mail address: zrguang@cug.edu.cn (R. Zuo).

http://dx.doi.org/10.1016/j.oregeorev.2015.12.005
0169-1368/

quantify spatial associations between evidence layers (or geological factors) and known mineral occurrences based on fuzzy sets and fuzzy probabilities. The FWofE method integrates the prior probability of mineral occurrences with the conditional probability for each evidential layer to obtain posterior probabilities of mineral occurrence. Instead of separating evidence into binary or ternary forms, this method allows objective or subjective definitions of fuzzy membership by relatively objective definitions of fuzzy or conditional probabilities. This effectively minimizes the uncertainty caused by missing data and improves the prediction accuracy, providing a powerful tool for measuring spatial correlations between spatial features (Cheng and Agterberg, 1999; Cheng and Zhang, 2002; Cheng et al., 2007).

The random forest (RF) method, which is a machine learning method based on a decision tree classifier (Breiman et al., 1984), is increasingly being applied to data-driven predictive mapping of mineral prospectivity. It is an ensemble classification scheme that uses a majority vote for class association based on the results of multiple decision trees (Cracknell and Reading, 2013). Reddy and Bonham-Carter (1991) used a decision-tree method to map mineral prospectivity for base-metal deposits in the Snow Lake area of Manitoba (Canada). Rodriguez-Galiano et al. (2014, 2015) applied the RF method to map gold prospectivity in southern Spain. Carranza and Laborte (2015a, 2015b, 2015c) tested the efficacy of an RF algorithm. Harris et al. (2015) utilized the RF method to map prospectivity in Canada's northern Melville Peninsula area. Furthermore, Zhang et al. (2015) chose southwestern Fujian Province in China as a case study area to compare the FWofE and RF methods for mapping mineral prospectivity for skarn-type Fe deposits. Mckay and Harris (2015) applied the RF for mapping gold prospectivity in southern Nunavut (Canada).

In this paper, both the FWofE and RF methods are used to map mineral prospectivity for Cu polymetallic mineralization in southwest Fujian

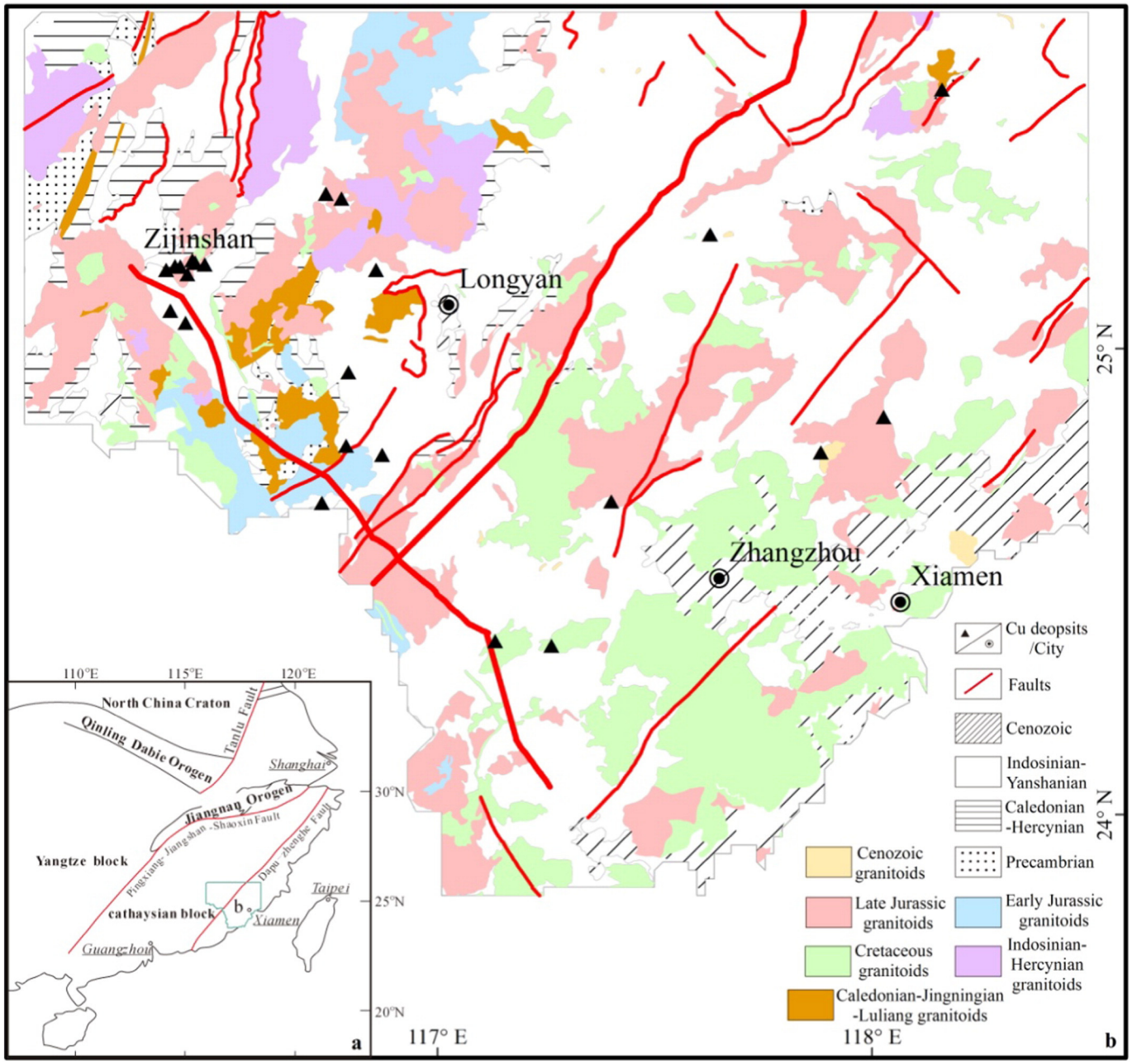

Fig. 1. Simplified geological map of southwestern Fujian Province (compiled from China Geological Survey, 2011).

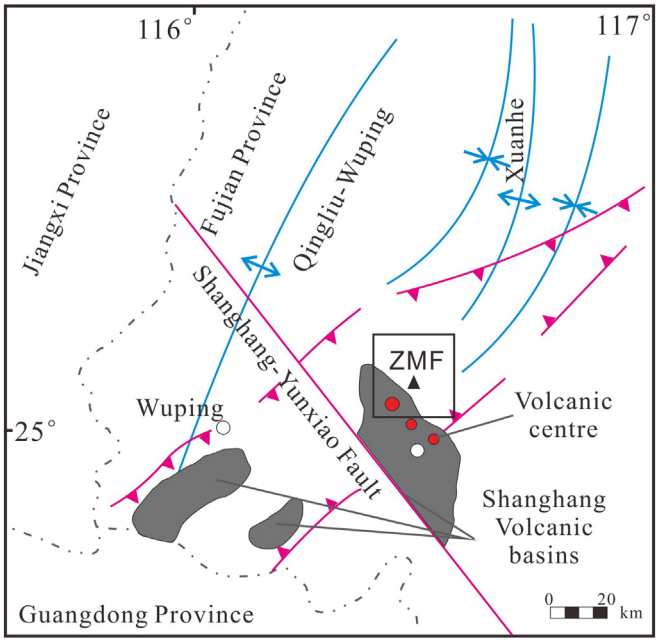

Fig. 2. Regional tectonic framework of the Zijinshan region (after Jiang et al., 2013).

Province. The aims of this study are: (1) to produce a prospectivity map for Cu polymetallic mineralization in southwest Fujian Province; and (2) to compare the FWofE and RF methods.

2. Data and methods

2.1. Data

The datasets used in this study consists of geological, geochemical, and geophysical data. A 1:200,000 geological map, including intrusive rocks, volcanic rock formations, faults, and mineral occurrences, was obtained from the China Geological Survey (CGS). Regional stream sediment geochemical data for 39 major and trace elements were collected from the Chinese National Geochemical Mapping (CNGM) project, initiated in 1979 (Xie et al., 1997). Xie et al. (1997) provide a more detailed description of the geochemical data, including analysis methods, data quality, and sampling strategy. The geophysical datasets consist of Bouguer gravity and airborne total magnetic data obtained from the CGS at 2 km spatial resolution.

2.2. Fuzzy weights of evidence

The FWofE method defines an evidence layer as a fuzzy set with a membership function consisting of multiple values, rather than the binary or ternary sets commonly involved in the ordinary WofE (Cheng and Agterberg, 1999). The binary and ternary patterns are special cases of the fuzzy set (e.g. μ(A) = 1 or 0 correspond to a binary pattern and μ(A) = 0, 0.5 and 1 correspond to a ternary pattern). Suppose that evidence X is related to hypothesis H regarding the occurrence of mineralization of type D, then $X=\{x_1,x_2,\cdots x_n\}$ consists of discrete states (continuous variables are separated into classes). In MPM, x_i can be defined as an anomalous class. Suppose that $A\subset X$ is the created fuzzy set, then the degree of each element x belonging to A can be described by a membership function $u_{A(x)}$ with the following properties:

(1) $0\le\mu_{A(x)}\le 1$,
(2) $\mu_{A(x)}=1$, *if and only if* $x\in A$,
(3) $\mu_{A(x)}=0$, *if and only if* $x\notin A$,

For convenience, let A_1 and A_2 denote the subsets

$$A_1=\left\{x;\ \mu_{A(x)}=1\right\},\quad A_2=\left\{x;\ \mu_{A(x)}=0\right\} \tag{1}$$

where $A_1\cup A_2\subset X$, $A_1\cap A_2=0$. The membership function then gives

$$\mu_{A(x)}=\frac{c-\min_{x\in A_2}c}{\max_{x\in A_1}c-\min_{x\in A_2}c} \tag{2}$$

where the contrast value c equals $W^+ - W^-$, and W^+ and W^- are calculated using the WofE method of Agterberg et al. (1993)

If A and B are conditionally independent of D, the natural logarithm of the probability of D for the two given fuzzy sets A and B can be expressed as:

$$\ln O\left[D\middle|\mu_{A(x)}\mu_{B(y)}\right]=\ln\frac{P\left[D\middle|\mu_{A(x)}\mu_{B(y)}\right]}{1-P\left[D\middle|\mu_{A(x)}\mu_{B(y)}\right]}=W_0+W_{\mu_{A(x)}}+W_{\mu_{B(y)}} \tag{3}$$

where the left side of Eq. (3) represents the natural logarithm of the odds of D given evidence that A. Functions $W_{u_A(x)}$ and $W_{u_B(y)}$ are weighted for the fuzzy sets A and B, and they can be expressed in terms of B with fuzzy membership functions $u_{A(x)}$ and $u_{B(y)}$, respectively. W_0 corresponds to the prior probability.

Functions:

$$W_{\mu_{A(x)}}=\ln\frac{P\left[\mu_{A(x)}|D\right]}{P\left[\mu_{A(x)}|\overline{D}\right]}=\ln\frac{\mu_{A(x)}P[A_1|D]+\left(1-\mu_{A(x)}\right)P[A_2|D]}{\mu_{A(x)}P\left[A_1|\overline{D}\right]+\left(1-\mu_{A(x)}\right)P\left[A_2|\overline{D}\right]} \tag{4}$$

$$W_{\mu_{B(y)}}=\ln\frac{P\left[\mu_{B(y)}|D\right]}{P\left[\mu_{B(y)}|\overline{D}\right]}=\ln\frac{\mu_{B(y)}P[B_1|D]+\left(1-\mu_{B(y)}\right)P[B_2|D]}{\mu_{B(y)}P\left[B_1|\overline{D}\right]+\left(1-\mu_{B(y)}\right)P\left[B_2|\overline{D}\right]} \tag{5}$$

Additional details for the FWofE method can be found in Cheng and Agterberg (1999).

2.3. The random forest method

Random forest (RF) is an ensemble machine learning method, originally developed by Breiman (2001), that combines multiple decision tree (DT) algorithms to classify or predict the value of variables (Breiman, 2001; Guo et al., 2011). Like other data-driven methods for MPM, the RF algorithm requires training data consisting of known mineral locations and no-deposit locations. To avoid the correlation of different trees, the RF method increases the diversity of the trees by growing them from different training data subsets created through a procedure called "bagging". Bagging is a technique used for obtaining training data for each decision tree by randomly sampling (with replacement) a number of samples equal to the number of instances in the training dataset, leading to the possibility that some data are used more than once during training, although other data may never be used. Each tree employs a bagging process known as "bootstrap sampling" in which approximately two-thirds of the training areas (or pixels) are randomly selected (with replacement) and used to generate the classification (in-bag data); the remaining one-third (out-of-bag or oob data) are used for validation. This random sampling (with replacement) of the training dataset is undertaken for every tree. The in-bag data are used to create multiple decision trees that are applied to produce independent classifications, and the oob data are used to validate the classification by calculating an oob error. Compared with cross-validation, the oob error is unbiased and provides a good estimate of the generalization error (Harris et al., 2015).

The Gini impurity index (Breiman et al., 1984) is used to determine the "optimal split" threshold at each node of a decision tree in the RF

algorithm. The Gini impurity index (I_G), which measures the impurity of an attribute with respect to the classes, is defined as:

$$I_G(f) = \sum_{i=1}^{m} f_i(1-f_i) \quad (6)$$

where f_i denotes the probability of class i at node m, defined as:

$$f_i = \frac{n_j}{n} \quad (7)$$

where n_j denotes the number of samples that belong to class j, and n is the total number of samples within a particular node. The attribute of the lowest I_G is used as the decision tree splitting criterion.

The RF method combines the prediction output of each RT algorithm using a rule-based approach (Breiman, 2001). For prediction, classifiers are combined by a majority vote from the outcome of k random decision trees within the forest, and the output of the RF is calculated by the equation:

$$P_j = \frac{1}{k}\sum_{j=1}^{k} y_j^i \quad (8)$$

where j denotes the possible classes of the sample (deposits and non-deposits when mapping mineral prospectivity) and y_j^i is the prediction result belonging to class j in the i-th decision tree.

RF provides additional information concerning the data as well as an accurate prediction, because of its random features. The following significant information is obtained from the oob data in the training dataset: (1) the error rate being approximately one-third of the prediction instances are omitted from the bootstrap, which can be set to obtain an unbiased estimate of the test set error rate (Breiman, 1996); and (2) the variable importance measures where the RF switches one of the input variables while retaining the remaining variables, and the output (mean squared error, or MSE) is given by the increased percentage of the oob rate divided by the misclassification rate (Breiman, 2001).

The RF method requires two training datasets. Usually, known mineral occurrences are used for positive cases. Other types of mineral occurrences and randomly selected points can be used for negative cases (Nykänen et al., 2015). Two parameters need to be set to generate a predictive model: the number of predictive variables (m) in the random subset at each node used to grow the decision tree and the number of classification trees (k). According to Breiman (2001), m should be less than $\log_2(M+1)$ (where M is the number of input variables) to minimize generalization error and correlation among decision trees. In this study, three forms of evidence were selected as input variables (M = 4), so m should be less than $\log_2(4+1)$ and m = int ($\log_2 4 + 1$) =

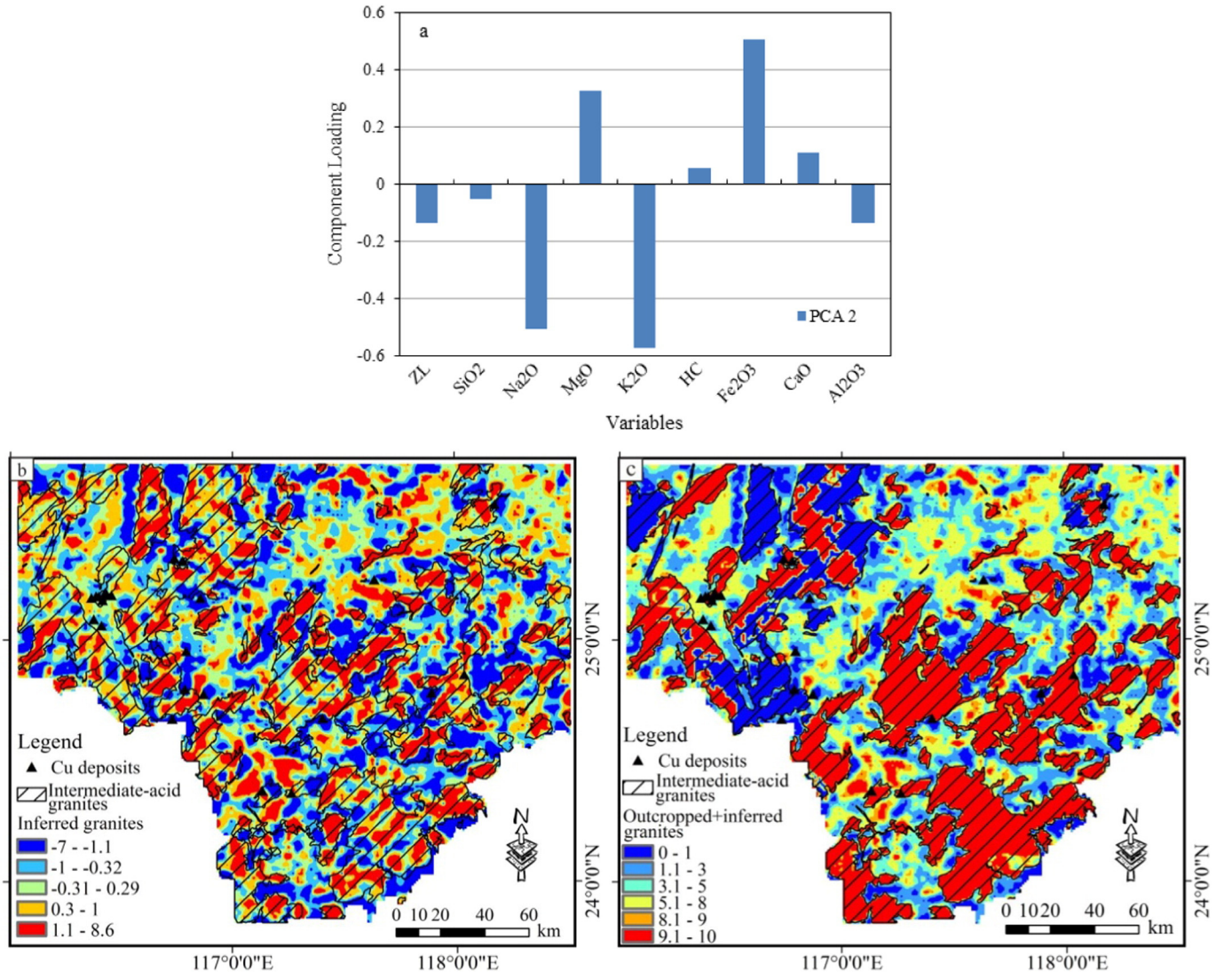

Fig. 3. Maps showing (a) loadings of PC2, (b) the spatial distribution of the PC2 score, and (c) the inferred Yanshannian intermediate-acid granites.

3. Rodriguez-Galiano et al. (2015) chose the Rodalquilar mining district as a case study area to test the application of the RF method to mineral prospectivity mapping, and they discussed the relationship between the number of trees (k) and the number of split variables (m). They concluded that using k = 1000 resulted in relatively low prediction errors and the most stable predictions.

2.4. Validation

There are a number of methods used to test the performance of prediction models, such as "cross-validation" (Agterberg and Bonham-Carter, 2005; Chung and Fabbri, 2008; Fabbri and Chung, 2008), "jack-knifing" (Bonham-Carter, 1994; Nykänen and Salmirinne, 2007), "receiver operating characteristics" (ROC) validation (Robinson and Larkins, 2007; Nykänen, 2008; Nykänen et al., 2015), and "prediction–area" (P–A) plots (Yousefi and Carranza, 2015a, 2015b, 2015c). In this study, P–A plots and ROC validation are addressed.

A P–A plot is constructed based on the ability of prospectivity models to predict mineral deposits with respect to the size of predicted target areas. It consists of: (1) the curve of prediction rate of the known mineral occurrences (on the left y-axis) corresponding to the classes of the weighted evidential map on the x-axis; and (2) the curve of percentage of occupied areas (on the right y-axis) corresponding to the classes of the weighted evidential map (Yousefi and Carranza, 2015b, 2015c). The intersection point defines the prediction rate in the P–A plot, which is a key criterion to evaluate and compare the different prospectivity models. This is because, if an intersection point appears at a higher place in the P–A plot, it indicates a smaller area containing a larger number of mineral deposits. Yousefi and Carranza (2015b) applied the normalized density to rank evidential layers and compared the prospectivity models. The normalized density can be expressed as $N_d = P_r/O_a$, where N_d is normalized density, and P_r and O_a are prediction rate and occupied area, respectively. More detailed information on the P–A plot can be found in Yousefi and Carranza (2015a, 2015b, 2015c).

The ROC graph is an alternative approach to visualizing, organizing, and selecting classifiers based on their performance (Egan, 1975; Fawcett, 2006; Swets and Monahan, 2000). Given a geochemical pattern with a total number of cells C, in which N cells are occupied by known mineral deposits (each cell is occupied by only one mineral deposit), P cells (equal to C–N) do not contain known mineral occurrences. For a given location, the four possible outcomes are: (1) if the location is occupied by a known mineral occurrence and is classified as a prospect (or an anomalous area), it is counted as a true positive (tp); (2) if the location is classified as a non-prospect (or background), it is counted as a false negative (fn); (3) if the location is occupied by no mineral deposits and is classified as a prospect, it is called a false positive (fp); and (4) if the location is classified as a non-prospect, it is called a true negative (tn). The true positive rate and the false positive rate can be calculated using the following equations:

$$\text{True positive rate} = \text{Prospectivities correctly classified}/N \quad (9)$$

$$\text{False positive rate} = \text{Non-prospectivities incorrectly classified}/P. \quad (10)$$

The paired data of (tp, fp) can be obtained using a series of thresholds to classify the geochemical pattern. ROC graphs can then be constructed with the tp and fp rates plotted on the Y and X axes, respectively. An advantage of ROC curves is that they are insensitive to changes in the class distribution. If the proportion of positive to negative instances changes in a test set, the ROC curve will not change (Fawcett, 2006). The area under the ROC curve (AUC) is an index that can be used to compare classifiers, and it provides a single scalar value representing the expected performance. The value of the AUC ranges from 0 to 1.0, and the larger the AUC, the better the performance. A ROC curve nearer to (0, 1), leading to a larger AUC value, represents a more efficient classification.

3. Geological background and mineral deposit model

3.1. Geological background

The Cathaysia Block of southeastern China is subdivided into the Cathaysia Interior (CI), the Cathaysia Fold Belt (CFB), and the Southeast Coastal Magmatic Belt (SCMB) (Xia et al., 2015). The case study area, southwestern Fujian Province, is located in the CFB and SCMB, and it is considered to be one of the key polymetallic belts in southern China (Zhang et al., 2001; Zhong et al., 2011; Liang et al., 2012; Huang et al., 2013; Jiang et al., 2013). The widespread plutonic rocks are Permo-Triassic (Indosinian) and Jurassic–Cretaceous (Yanshanian) plutons with some Early Devonian (Caledonian) and Permian (Hercynian) plutons (Huang et al., 2013; Jiang et al., 2013) (Fig. 1). The Zijinshan mineral field (ZMF) is one of the most famous Cu polymetallic districts in southwestern Fujian Province, and it is located in the eastern part of the Cathaysia Fold Belt, at the intersection of the Xuanhe Anticlinorium and the Yunxiao–Shanghang Fault, and at the northeastern margin of the Cretaceous Shanghang Volcanic Basin (Zhong et al., 2011; Liang et al., 2012; Huang et al., 2013; Jiang et al., 2013) (Fig. 2). The Cu polymetallic mineralization in the area is generally associated with Jurassic to Cretaceous granitic plutons (e.g. the Sifang Granite and Caixi

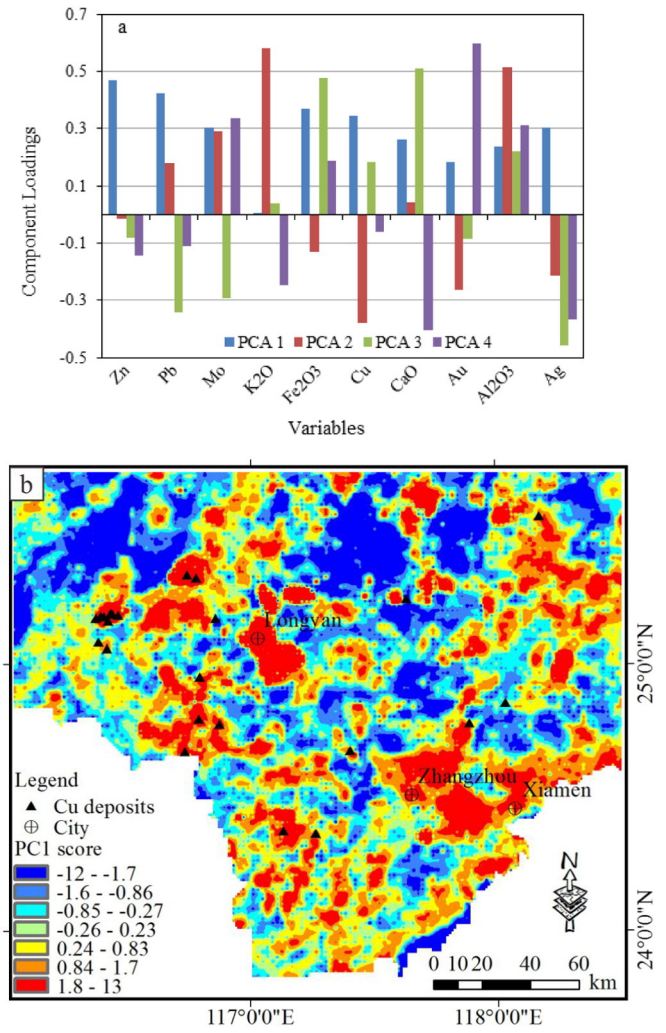

Fig. 4. Maps showing (a) loadings of geochemical variables on principal components, and (b) the spatial distribution of PC1 scores.

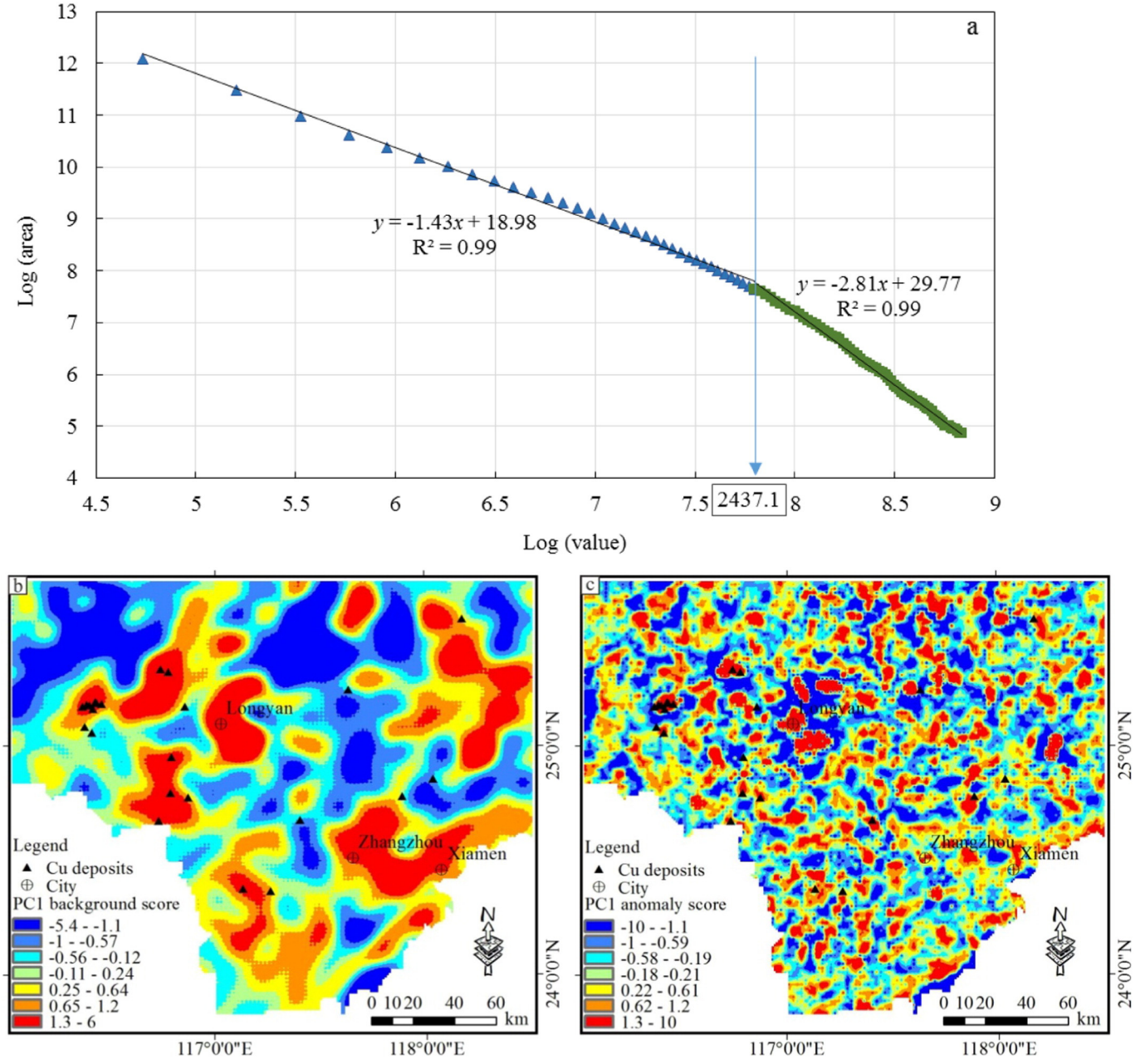

Fig. 5. Maps showing (a) S–A plot, (b) the background component of PC1, and (c) the anomaly component of PC1.

Granite) and mafic volcanic rocks (Zhong et al., 2011). The lithostratigraphic units in the ZMF include Early Cretaceous volcanic assemblages assigned to the Shimaoshan Group in the southwest, which underwent high-level uplift and erosion during the Cenozoic, and Neoproterozoic to Carboniferous metamorphic and clastic rocks distributed in the northwest. Middle to Late Jurassic and Early Cretaceous plutons host most of the orebodies in the area, and they were formed by multistage intrusions, including the Middle Jurassic Zijinshan Granite, the Late Jurassic Caixi Monzogranite, the Early Cretaceous Sifang Granodiorite, and small-sized granitic porphyries, dacite porphyries, and cryptoexplosive breccia pipes (Zhong et al., 2014). These features characterize the Jurassic and Cretaceous magmatic events in the ZMF.

3.2. Ore geology

The Zijinshan Cu–Au deposit is the first occurrence of a high sulfidation-type epithermal deposit identified in mainland China and is discovered in the late 1980s (So et al., 1998). The Cu–Au mineralization in the ZMF ranges from high-sulfidation epithermal to porphyry types, and is characterized by NW-trending breccia bodies and veins in a Cretaceous volcanic pipe (Pirajno and Bagas, 2002). By the end of 2008, Zijinshan, containing 2.36 Mt. Cu at an average grade of approximately 0.45%, was the leading Cu producer in the Fujian Province (Zhong et al., 2014). Copper deposits in the mineral field can be grouped into epithermal (e.g. Zijinshan), porphyry (e.g. Luobuling), and transitional epithermal and porphyry (e.g. Wuziqilong) types (So et al., 1998).

Both gold and copper orebodies are distinctly zoned at Zijinshan, with gold mineralization in the upper mine levels and copper at deeper levels. Most of the mineralization at the deposit is in an alunite alteration zone located below 650 m, hosted by NW-trending breccia bodies and veins within a Cretaceous dacitic porphyry volcanic pipe (Jiang et al., 2013). Hydrothermal alteration and mineralization are typically zoned with a quartz–sericite–pyrite assemblage in the deeper to outer

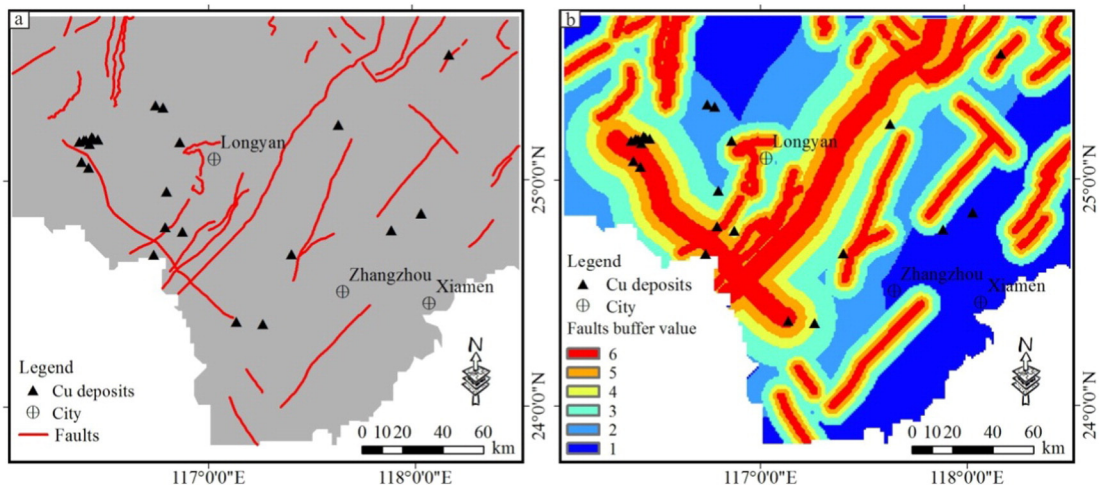

Fig. 6. Maps showing (a) faults and (b) buffer zones of faults.

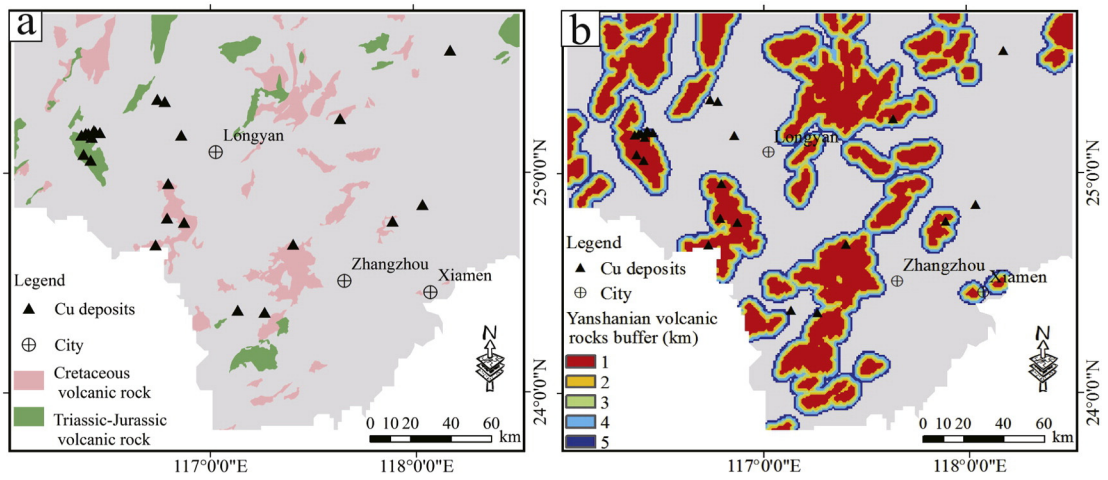

Fig. 7. Maps showing (a) Yanshannian volcanic rock formations and (b) buffer zones of Yanshannian volcanic rocks.

parts of the system at depths between 350 and 1200 m, a dickite–quartz–pyrite–zunyite assemblage at middle levels, and alunite–quartz–pyrite nearer to the ground surface. Metal zoning within the alunite–quartz–pyrite zone progresses from Cu–Pb–Zn to Au–Ag–As near the ground surface (Pirajno and Bagas, 2002).

The Cu mineralization in the ZMF is related to Early Cretaceous granodiorite and volcanic rocks. These igneous rocks crop out in the central–southern and northeastern parts of the mineral field, where they are located in northwest-trending structures linked to the deep-seated Yunxiao–Shanghang Fault (Zhang et al., 2001). The Sifang Granodiorite is the youngest Cretaceous intrusion in the ore district and consists of fine- to medium-grained granodiorite elongated in a NNE-trending direction (Mao et al., 2002). The granodiorite intrudes Neoproterozoic metamorphic rocks, Devonian–Carboniferous clastic rocks and limestone, and the Zijinshan Granite. Dacitic porphyry hosts Cu–Au mineralization at the Zijinshan deposit, whereas granodioritic porphyry hosts Cu–Mo mineralization at the Luoboling deposit (Zhang et al., 2005).

The pre-Jurassic rocks in the ZMF are folded into a NE-trending anticline that is intruded by the Jurassic to Cretaceous plutons. Previous studies have shown that the NE-trending faults that formed during compression and shearing controlled the emplacement of the Jurassic granites, whereas the NW-trending faults that are mainly tensional are associated with Early Cretaceous magmatism and Cu–Au mineralization (So et al., 1998; Xue and Ruan, 2008; Wang et al., 2009). The plutons host most of the orebodies in the area and were formed by multistage granitic intrusions, including the: (1) Middle Jurassic Zijinshan Granite with a sensitive high-resolution ion microprobe (SHRIMP) U–Pb zircon age of

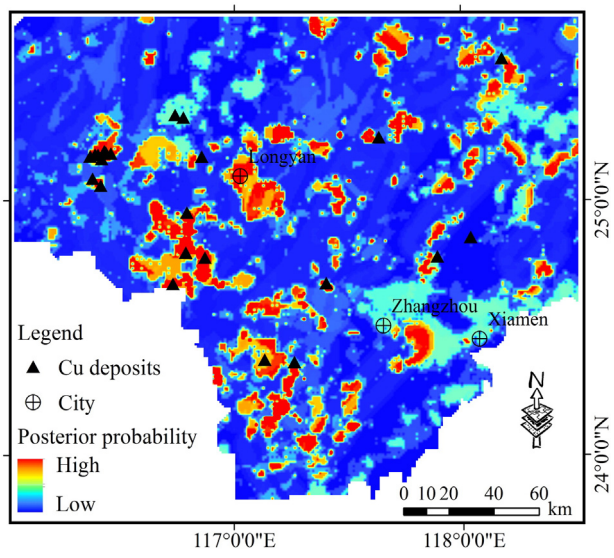

Fig. 8. Probability map obtained by FWofE.

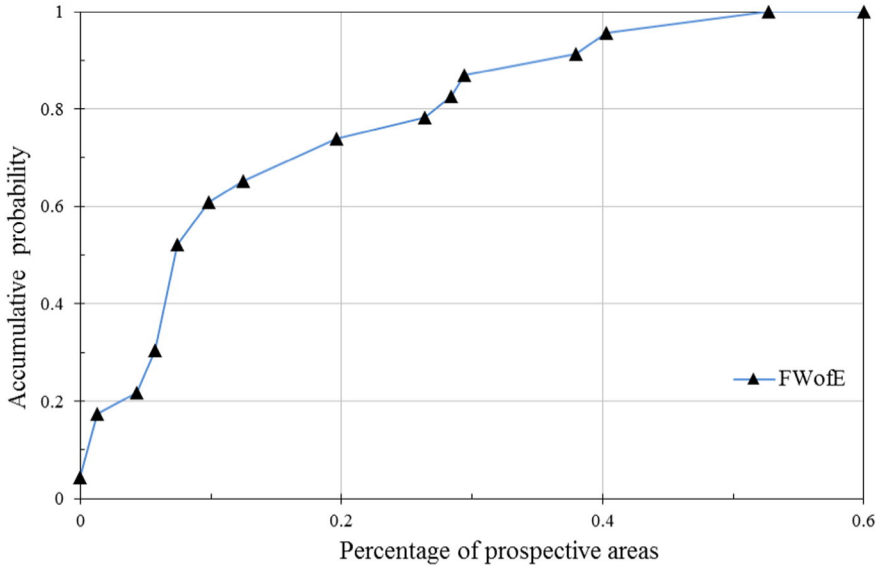

Fig. 9. Plot of accumulative prospective areas versus accumulative probability obtained by FWofE.

168 ± 4 Ma (Zhao et al., 2008) and a laser ablation inductively coupled plasma mass spectrometry (LA-ICP-MS) U–Pb zircon age of 165 to 157 Ma (Jiang et al., 2013); (2) Late Jurassic Caixi monzogranitic pluton with a SHRIMP U–Pb zircon age of 150 ± 3 Ma (Zhao et al., 2007); (3) Early Cretaceous Sifang Granodiorite with a SHRIMP U–Pb zircon age of 108 ± 1 Ma, a hornblende Ar–Ar plateau age of 105 ± 1 Ma (Mao et al., 2002), an LA–ICP–MS U–Pb zircon age of 112 ± 1 Ma (Jiang et al., 2013); and (4) small-sized granitic porphyries, dacite porphyries, and cryptoexplosive breccia pipes. It is noteworthy that the breccia pipes and porphyries are spatially, temporally, and genetically relationed with the mineral systems.

4. Mapping evidence

The Cu mineralization is genetically related to the Early Cretaceous granodiorite and volcanic rock formations. These igneous rocks outcrop in the central–southern and northeastern parts of the ZMF, where they are located in NW-trending structures linked to the deep-seated Yunxiao–Shanghang Fault. Four key geological factors were selected as important criteria for mapping Cu polymetallic mineralization in southwest Fujian Province: (1) Jurassic to Cretaceous granodiorite, (2) geochemical anomalies related to Cu polymetallic mineralization processes, (3) NE- and NW-trending faults, and (4) Jurassic to Cretaceous volcanic rocks.

4.1. Jurassic to Cretaceous granodiorite

The Jurassic to Cretaceous granodioritic intrusions play an important role in the Cu polymetallic mineralization in the study area (Jiang et al., 2013). Although the outcrop of the intrusions has already been mapped in the study area, using only outcropped sections as an evidential layer for mapping Cu polymetallic mineralization, which may lead to

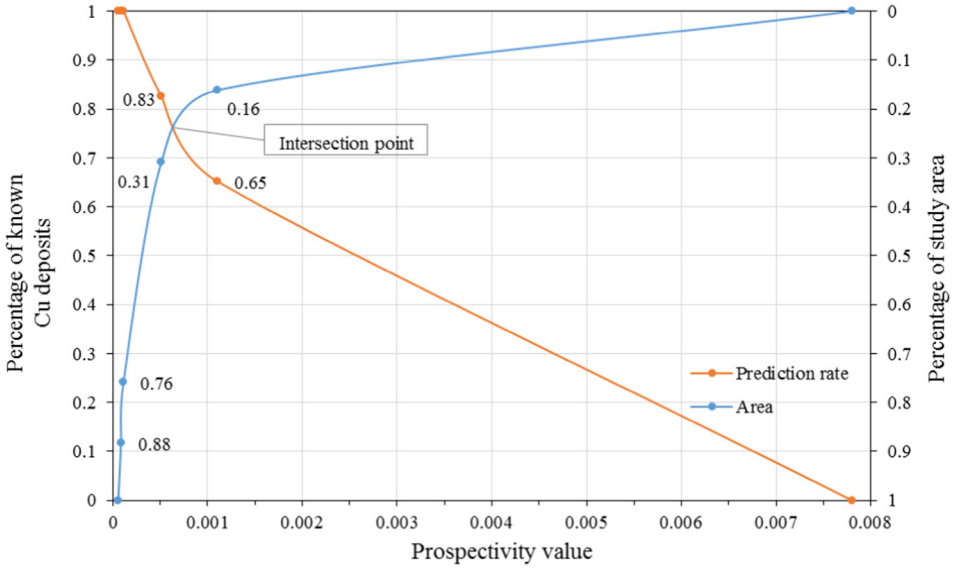

Fig. 10. Prediction–area (P–A) plot for the FWofE prospectivity model.

uncertainties resulting from granodioritic intrusions of that age that might be present in the study area. Therefore, the inferred intrusions were classified based on the distinguishing mineralogical and geochemical features of the magmatic, sedimentary, and metamorphic rocks. Mafic magmatic rocks are always characterized by higher concentrations of elements such as MgO, Fe_2O_3 and CaO compared with felsic magmatic rocks, which have higher concentrations of elements such as K_2O, Na_2O, SiO_2 and Al_2O_3. Intermediate to felsic intrusive rocks always exhibit low gravity anomalies and weak magnetic anomalies compared with sedimentary and metamorphic rocks (Cheng, 2012). Therefore, major element geochemical data (K_2O, Na_2O, SiO_2, Al_2O_3, MgO, Fe_2O_3, and CaO) and geophysical data were used to infer the location of the Jurassic to Cretaceous granodioritic intrusions in the study area. Based on the available spatial datasets, the Jurassic to Cretaceous granodioritic intrusions were distinguished from all of the exposed rocks in the study area. The spatial interpolation for the major element geochemical data was processed using the inverse distance weighted (IDW) method, with a spatial resolution of 1 km. To reduce the asymmetry of the magnetic field caused by the geomagnetic inclination and declination, the original aeromagnetic data were preprocessed to reduce the geomagnetic pole; oblique magnetization was transformed to vertical magnetization (Cooper and Cowan, 2005).

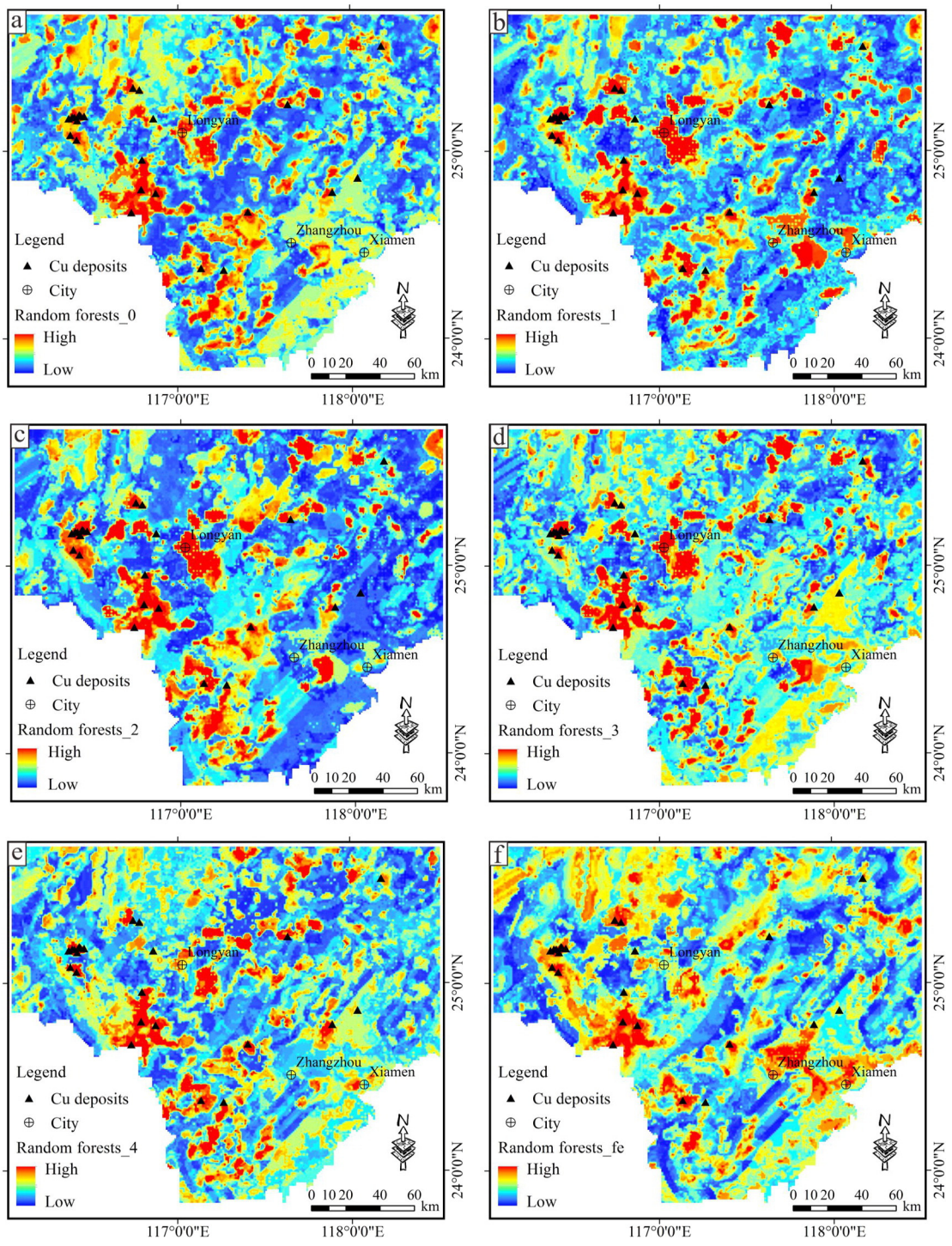

Fig. 11. Probability maps obtained by RF.

The local singularity analysis developed by Cheng (2007) was used to process the geochemical and geophysical data. The major geochemical and geophysical anomalies were generated using principal component analysis (PCA), which is one of the most popular methods of multivariate analysis used to reduce the dimensionality of datasets producing relatively few unrelated principal components based on covariance or correlations of variables (Jolliffe, 2002). The resulting PCA in Fig. 3a shows that PC2 consists of positive loadings for MgO (0.33), Fe_2O_3 (0.51), and CaO_3 (0.11), aeromagnetic anomalies (0.06), negative loadings of K_2O (−0.57), Na_2O (−0.50), Al_2O_3 (−0.14), and SiO_2 (−0.05), and gravity anomalies (−0.14), indicating that a negative PC2 is an indicator for intermediate–acid intrusions. The spatial distribution of PC2 in Fig. 3b shows a strong spatial correlation with the mapped granitic intrusions. The inferred and outcrop intrusions were integrated in Fig. 3c as an evidential layer for mapping mineral prospectivity.

4.2. Geochemical anomalies

Ten alteration- and mineralization-related elements (Cu, Au, Fe, Pb, Zn, Al, Ag, Mo, K, and Ca) were chosen to map geochemical anomalies associated with Cu mineralization in ZMF. To obtain a composite geochemical map, the aforementioned elements were processed using the IDW method and integrated using PCA. The PCA results revealed that PC1 is composed of positive loadings from Cu, Au, Fe, Pb, Zn, Al, Ag, Mo, K, and Ca and that 36.8% of the total variance was retained in PC1 (Fig. 4a). The PC1 possibly represents Cu polymetallic mineralization associated with intrusions and NE- and NW-trending faults, which exhibit a strong spatial distribution with the known Cu polymetallic deposits (Fig. 4b).

The spectrum–area (S–A) multifractal model developed by Cheng et al. (1999, 2000) is considered to be a sophisticated and useful technique for decomposing mixed geochemical patterns (Cheng, et al., 1999, 2012; Zuo, 2011, 2014; Zuo et al., 2013; Zuo and Wang, 2015). In this study, the S–A method was applied to process the mixed geochemical data, separating background and anomalous areas. A Fourier transform (FT) was used to convert the PC1 score map from the spatial domain into the frequency domain. A pair of datasets consisting of the power spectrum density (S) and the area with power spectrum density was obtained and plotted on a log–log graph, allowing the datasets to be fitted by two straight lines using the least squares (LS) method. A cut-off value (S = 2437.1) is observed in Fig. 5a. The left-hand part of this figure shows the straight-line fit $y = -1.43\times + 18.98$ ($R^2 = 0.99$), which is considered anomalous ($S \le 2437.1$). The right-hand part shows the straight-line $y = -2.82\times + 29.77$ ($R^2 = 1.00$), which represents the background data ($S > 2437.1$). These two parts were then transformed back to the spatial domain via an inverse Fourier transformation, and background and anomaly maps were obtained (Fig. 5b, c). The anomaly map shows that highly anomalous areas have a strong spatial correlation with known Cu deposits in the study area.

4.3. NE- and NW-trending faults

Porphyry–epithermal deposits in ZMF are closely and indirectly associated with regional deep (first-order) faults interpreted as pathways for mineralizing fluids, with the majority of the mineral occurrences distributed along secondary (or second-order) fault systems (Halter et al., 2004). Both the NE-trending Zhenghe–Dapu and the NW-trending Shanghang–Yunxiao fault (Chen et al., 2015), which are conspicuous geological structures in the study area, as well as a series of NE- and NW-trending faults, were extracted from the geological maps of the study area (Fig. 6a). A multi-ring buffer around the regional deep faults was constructed using an interval of 5 km for 10 rings, and around the secondary faults using an interval of 2 km for 5 rings (Fig. 6b).

4.4. Jurassic to Cretaceous volcanic rocks

The ZMF is located in the northeastern margin of the Cretaceous Shanghang Volcanic Basin where Jurassic to Cretaceous volcanic rocks and granodiorite host the Cu polymetallic mineralization, which show a close spatial relationship with the known Cu polymetallic occurrences. The mineralization ranges from high-sulfidation epithermal- to porphyry-types, and the area is characterized by NW-trending breccia bodies and veins within a volcanic pipe (Jiang et al., 2013). Therefore, the volcanic rocks were selected as an important criterion for mapping mineral prospectivity. Fig. 7a shows the spatial distribution of the volcanic rocks in the study area and demonstrates a strong spatial correlation between them and known Cu deposits, and Fig. 7b shows the buffer zones of the volcanic rocks.

5. Results and discussion

To obtain the posterior probabilities, 23 known porphyry–epithermal Cu deposits were selected in ZMF as training data for calculating the fuzzy weights for all evidential layers using the FWofE method in support by GeoDAS GIS (Cheng, 2000). The results showed that the known Cu deposits are located in or near areas with high values of posterior probability (Fig. 8). To evaluate the success rate of the predictions, a plot of accumulative prospective areas against accumulative probability for Cu deposits was constructed, and it shows that 10% of the total study area contains approximately 60% of the total known Cu deposits (Fig. 9).

To evaluate the performance of the FWofE model generated in this study, 23 known porphyry–epithermal Cu deposits were selected as

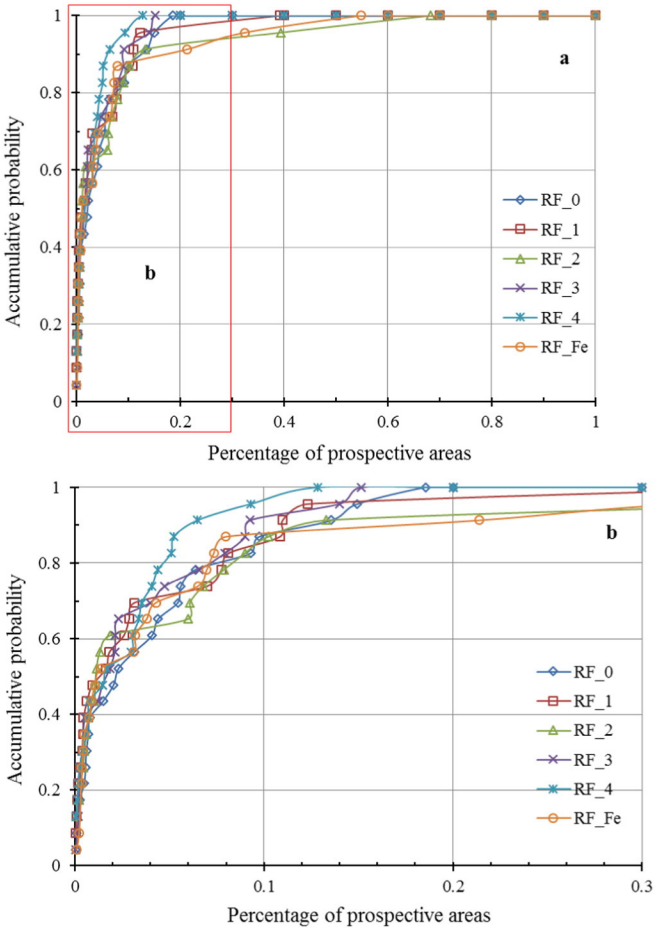

Fig. 12. Plots of accumulative prospective areas versus accumulative probability obtained by RF.

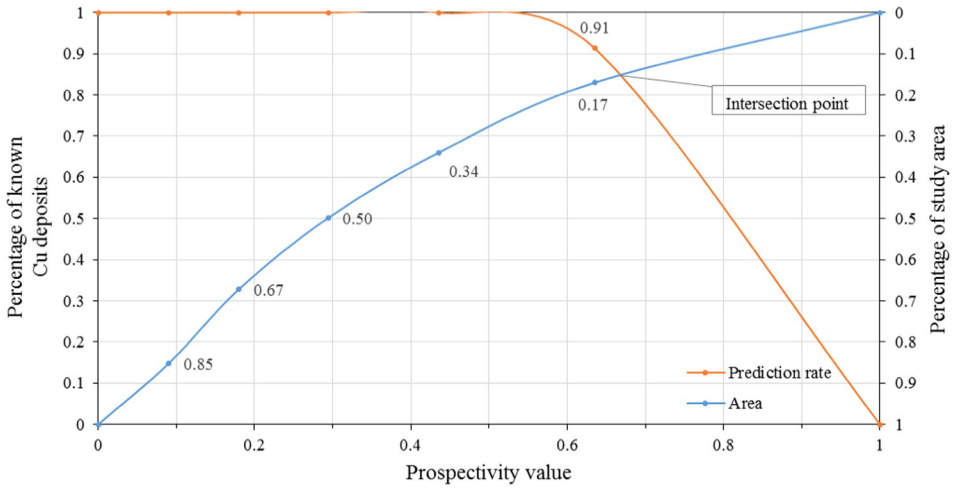

Fig. 13. Prediction–area (P–A) plot for the RF prospectivity model.

testing points to create a P–A plot. The results show that the normalized density is 3.17 and its weight is 1.15 (Fig. 10).

In this study, a set of 23 known Fe deposits and five sets of 23 random points in the region were selected as negative cases. By comparing six probability maps obtained using the RF method with known Cu deposits (Fig. 11), it can be observed that most of the known Cu deposits are situated in the high probability region. The curves of RF (0–4) and RF (Fe) show that approximately 15% of the total area contains more than 90% of the known Cu deposits (Fig. 12), indicating a good performance for the RF method. The RF0 is selected to construct a P–A plot, and the results show that the normalized density is 5.25 and its weight is 1.66 (Fig. 13).

The RF method represents a type of machine learning. Overfitting often happens when a model memorizes and can perfectly predict the training data, but the model generally shows poor predictive performance because it can exaggerate minor fluctuations in the data. To avoid overfitting, it is necessary to test the model's ability by evaluating its performance on a set of data not used for training. Therefore, the ROC graph was used to test the performance of the predictive model for Cu polymetallic deposits. Twenty-three known Cu deposits and a set of random points were selected as true positive and true negative cases, respectively. The results showed that: (1) the AUC values from the RF and the FWofE methods were higher than 0.5, indicating that these two methods are useful for mapping Cu mineral prospectivity; and

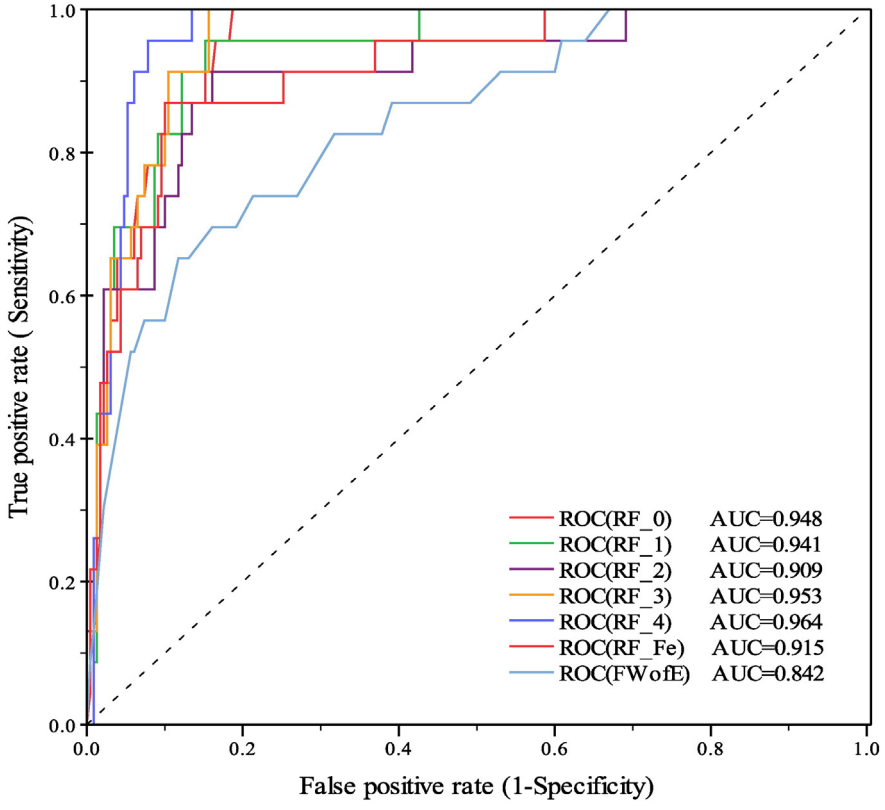

Fig. 14. ROC curves.

(2) the AUC value from the RF method was greater than that from the FWofE, suggesting a better performance by the RF method in this study (Fig. 14).

6. Conclusions

In this study, both the FWofE and RF methods were used to map mineral prospectivity for Cu polymetallic mineralization in southwestern Fujian Province, China. The following conclusions were obtained.

Both predictive maps obtained using the FWofE and RF methods showed highly successful prediction ratios, and the small target areas contained most of the known Cu deposits, indicating that a predictive model consisting of four evidence layers is powerful for mapping mineral prospectivity for Cu polymetallic deposits. These predictive maps can provide useful information for the next round of mineral explorations in the study area.

The P–A plots show that the normalized density (1.66) of RF is larger than that of FWofE (1.15), indicating that RF performs better than FWofE in this study. The AUC value of the RF map is higher than that of the FWofE map, also indicating a better performance of RF.

Other types of mineral deposits and randomly selected points provide alternative approaches for mapping mineral prospectivity, as they indicate non-prospectivity, and they can be used to check the effects of overfitting.

Acknowledgments

The authors thank Dr. Leon Bagas (associate editor), Dr. John Carranza and Dr. Mahyar Yousefi for their comments and suggestions, which improve this study. This research benefited from the National Natural Science Foundation of China (Nos. 41522206 and 41372007).

References

Agterberg, F.P., 1971. A probability index for detecting favourable geological environments. Can. Inst. Min. Metall. 10, 82–91.
Agterberg, F.P., 1973. Probabilistic models to evaluate regional mineral potential. Mathematical methods in Geoscience. Symposium held at Pribram, Czechoslovakia, pp. 3–38.
Agterberg, F.P., 1974. Automatic contouring of geological maps to detect target areas for mineral exploration. Math. Geol. 6, 373–395.
Agterberg, F.P., 1989. Computer programs for mineral exploration. Science 245, 76–81.
Agterberg, F.P., Bonham-Carter, G.F., 2005. Measuring the performance of mineral-potential maps. Nat. Resour. Res. 14, 1–17.
Agterberg, F.P., Bonham-Carter, G.F., Wright, D.F., 1990. Statistical pattern integration for mineral exploration and assessment for metals and petroleum. Pergamon Press, Oxford–New York (1–21 pp).
Agterberg, F.P., Bonham-Carter, G.F., Cheng, Q., Wright, D.F., 1993. Weights of evidence modeling and weighted logistic regression for mineral potential mapping. Comput. Geol. 25, 13–32.
An, P., Moon, W.M., Rencz, A., 1991. Application of fuzzy set theory for integration of geological, geophysical and remote sensing data. Can. J. Explor. Geophys. 27, 1–11.
An, P., Moon, W.M., Bonham-Carter, G.F., 1994. Uncertainty management in integration of exploration data using the belief function. Nat. Resour. Res. 3, 60–71.
Bonham-Carter, G.F., 1994. Geographic Information Systems for Geoscientists: Modeling with GIS. Pergamon Press, Ontario, Canada, p. 398.
Bonham-Carter, G.E., Cox, S., 1995. Geographic information systems for geoscientists: modelling with GIS. Econ. Geol. Bull. Soc. Econ. Geol. 90, 1352–1353.
Bonham-Carter, G.F., Agterberg, F.P., Wright, D.F., 1990. Weights of evidence modelling: A new approach to mapping mineral potential. Geol. Surv. Can. Pap. 89–9.
Breiman, L., 1996. Bagging predictors. Mach. Learn. 24, 123–140.
Breiman, L., 2001. Random forests. Mach. Learn. 45, 5–32.
Breiman, L., Friedman, J.H., Olshen, R.A., Stone, C.J., 1984. Classification and regression trees. Boca Raton. Journal of Beijing Normal University 38, 15–22.
Brown, W.M., Gedeon, T.D., Groves, D.I., Barnes, R.G., 2000. Artificial neural networks: a new method for mineral prospectivity mapping. Aust. J. Earth Sci. 47, 757–770.
Carranza, E.J.M., 2009. Geochemical anomaly and mineral prospectivity mapping in GIS. Handbook of Exploration and Environmental Geochemistry vol. 11. Elsevier, Amsterdam (351 pp).
Carranza, E.J.M., 2011. Geocomputation of mineral exploration targets. Comput. Geosci. 37, 1907–1916.
Carranza, E.J.M., Laborte, A.G., 2015a. Data-driven predictive mapping of gold prospectivity, Baguio district, Philippines: application of random forests algorithm. Ore Geol. Rev. 71, 777–787.
Carranza, E.J.M., Laborte, A.G., 2015b. Random forest predictive modeling of mineral prospectivity with small number of prospects and data with missing values in Abra (Philippines). Comput. Geosci. 74, 60–70.
Carranza, E.J.M., Laborte, A.G., 2015c. Data-driven predictive modeling of mineral prospectivity using random forests: a case study in Catanduanes Island (Philippines). Nat. Resour. Res. http://dx.doi.org/10.1007/s11053-015-9268-x.
Carranza, E.J.M., Mangaoang, J.C., Hale, M., 1999. Application of mineral exploration models and GIS to generate mineral potential maps as input for optimum land-use planning in the Philippines. Nat. Resour. Res. 8, 165–173.
Carranza, E.J.M., Woldai, T., Chikambwe, E.M., 2005. Application of data-driven evidential belief functions to prospectivity mapping for a quamarine-bearing pegmatites, Lundazi District, Zambia. Nat. Resour. Res. 14, 47–63.
Chen, J., Chen, Y., Zhong, J., Sun, Y., Qi, J., Li, J., 2015. Geological and ore–fluid characteristics of Longjiangting Cu deposit in Zijinshan Orefield, Fujian Province, and their genetic implications. Mineral Deposits 34, 98–118 (In Chinese with English Abstract).
Cheng, Q., 2000. GeoData Analysis System (GeoDAS) for Mineral Exploration: User's Guide and Exercise Manual. Material for the Training Workshop on GeoDAS Held at York University, Toronto, Canada (204 pp).
Cheng, Q., 2012. Singularity theory and methods for mapping geochemical anomalies caused by buried sources and for predicting undiscovered mineral deposits in covered areas. J. Geochem. Explor. 122, 55–70.
Cheng, Q., 2007. Mapping singularities with stream sediment geochemical data for prediction of undiscovered mineral deposits in Gejiu, Yunnan Province. China. Ore Geol. Rev. 32, 314–324.
Cheng, Q., Agterberg, F.P., 1999. Fuzzy weights of evidence method and its application in mineral potential mapping. Nat. Resour. Res. 8, 27–35.
Cheng, Q., Zhang, S., 2002. Fuzzy weights of evidence method implemented in GeoDAS GIS for information extraction and integration for prediction of point events. IEEE 2933–2935.
Cheng, Q., Chen, Z., Ali, K., 2007. Application of fuzzy weights of evidence method in mineral resource assessment for gold in Zhenyuan district, Yunnan Province, China. Earth Sci. 32, 175–184 (in Chinese with English abstract).
Chung, C., Fabbri, A.G., 2008. Predicting landslides for risk analysis spatial models tested by a cross-validation technique. Geomorphology 94, 438–452.
Cooper, G.R.J., Cowan, D.R., 2005. Differential reduction to the pole. Comput. Geosci. 31, 989–999.
Cracknell, M., Reading, A., 2013. The upside of uncertainty: identification of lithology contact zones from airborne geophysics and satellite data using random forests and support vector machines. Geophysics 78, WB113–WB126.
Egan, J.P., 1975. Signal Detection Theory and ROC Analysis. J. Comput. Syst. Sci. 40, 451-451.
Fabbri, A.G., Chung, C., 2008. On blind tests and spatial prediction models. Nat. Resour. Res. 17, 107–118.
Fawcett, T., 2006. An introduction to ROC analysis. Pattern Recogn. Lett. 27, 861–874.
Ford, A., Miller, J.M., Mol, A.G., 2015. A comparative analysis of weights of evidence, evidential belief functions, and fuzzy logic for mineral potential mapping using incomplete data at the scale of investigation. Nat. Resour. Res. http://dx.doi.org/10.1007/s11053-015-9263-2.
Geranian, H., Tabatabaei, S.H., Asadi, H.H., Carranza, E.J.M., 2015. Application of discriminant analysis and support vector machine in mapping gold potential areas for further drilling in the Sari-Gunay Gold Deposit, NW Iran. Nat. Resour. Res. http://dx.doi.org/10.1007/s11053-015-9271-2.
Guo, L., Chehata, N., Mallet, C., Boukir, S., 2011. Relevance of airborne lidar and multispectral image data for urban scene classification using Random Forests. J. Photogramm. Remote Sens. 66, 56–66.
Halter, W.E., Bain, N., Becker, K., Heinrich, C.A., Landtwing, M., VonQuadt, A., Clark, A.H., Sasso, A.M., Bissig, T., Richard, M.T., 2004. From andesitic volcanism to the formation of a porphyry Cu–Au mineralizing magma chamber: the Farallón Negro Volcanic Complex, northwestern Argentina. J. Volcanol. Geotherm. Res. 136, 1–30.
Harris, D.P., 1965. An Application of Multivariate Statistical Analysis to Mineral Exploration.
Harris, D.P., 1969. Alaska's base and precious metals resources: a probabilistic regional appraisal. Q. J. Colorado Sch. Min. 64, 295–327.
Harris, J.R., Grunsky, E., Behnia, P., Corrigan, D., 2015. Data-and knowledge-driven mineral prospectivity maps for Canada's North. Ore Geol. Rev. 71, 788–803.
Huang, W., Li, J., Liang, H., Wang, C., Lin, S., Wang, X., 2013. Zircon LA-ICP-MS U–Pb ages and highly oxidized features of magma associated with Luoboling porphyry Cu–Mo deposit in Zijinshan ore field, Fujian province. Acta Petrol. Sin. 29, 283–293 (in Chinese with English abstract).
Jiang, S., Liang, Q., Bagas, L., Wang, S., Nie, F., Liu, Y., 2013. Geodynamic setting of the Zijinshan porphyry–epithermal Cu–Au–Mo–Ag ore system, SW Fujian Province, China: Constrains from the geochronology and geochemistry of the igneous rocks. Ore Geol. Rev. 53, 287–305.
Jolliffe, I.T., 2002. Principal component analysis. second ed. Springer, New York, 547 NY (487 pp).
Liang, Q., Jiang, S., Wang, S., Li, C., Zeng, F., 2012. Re–Os dating of molybdenite from the Luoboling porphyry Cu–Mo deposit in the Zijinshan ore field of Fujian province and its geological significance. Acta Petrol. Sin. 86, 1113–1118 (in Chinese with English abstract).
Liu, Y., Cheng, Q., Xia, Q., Wang, X., 2014. Mineral potential mapping for tungsten polymetallic deposits in the Nanling metallogenic belt, South China. J. Earth Sci. 25, 689–700.
Mao, J., Tao, K., Lee, C., Xie, F., Xu, N., 2002. Geochronology and geochemical characteristics in late Mesozoic Sifang pluton, southwestern Fujian, and their significance. Acta Petrol. Sin. 18, 449–458 (in Chinese with English abstract).
Mckay, G., Harris, J.R., 2015. Comparison of the data-driven random forests model and a knowledge-driven method for mineral prospectivity mapping: a case study for gold

deposits around the Huritz Group and Nueltin Suite, Nunavut, Canada. Nat. Resour. Res. http://dx.doi.org/10.1007/s11053-015-9274-z.
Nykänen, V., 2008. Radial basis functional link nets used as a prospectivity mapping tool for orogenic gold deposits within the Central Lapland Greenstone Belt, Northern Fennoscandian Shield. Nat. Resour. Res. 17, 29–48.
Nykänen, V., Salmirinne, H., 2007. Prospectivity analysis of gold using regional geophysical and geochemical data from the Central Lapland Greenstone Belt, Finland. Geol. Surv. Finland 44, 251–269.
Nykänen, V., Lahti, I., Niiranen, T., Korhonen, K., 2015. Receiver operating characteristics (ROC) as validation tool for prospectivity models–a magmatic Ni–Cu case study from the Central Lapland Greenstone Belt, Northern Finland. Ore Geol. Rev. 71, 853–860.
Oh, H., Lee, S., 2010. Application of artificial neural network for gold-silver deposits potential mapping: a case study of Korea. Nat. Resour. Res. 19, 103–124.
Pirajno, F., Bagas, L., 2002. Gold and silver metallogeny of the South China fold belt: a consequence of multiple mineralizing events? Ore Geol. Rev. 20, 109–126.
Porwal, A., Carranza, E.J.M., 2015. Introduction to the special issue: GIS–based mineral potential modelling and geological data analyses for mineral exploration. Ore Geol. Rev. 71, 477–483.
Porwal, A., Carranza, E.J.M., Hale, M., 2006. A hybrid fuzzy weights-of-evidence model for mineral potential mapping. Nat. Resour. Res. 15, 1–14.
Reddy, R., Bonham-Carter, G.F., 1991. A decision-tree approach to mineral potential mapping in Snow Lake area, Manitoba. Can. J. Remote. Sens. 17, 191–200.
Robinson, G.R., Larkins, P.M., 2007. Probabilistic prediction models for aggregate quarry siting. Nat. Resour. Res. 16, 135–146.
Rodriguez-Galiano, V., Chica-Olmo, M., Chica-Rivas, M., 2014. Predictive modelling of gold potential with the integration of multisource information based on random forest: a case study on the Rodalquilar area, Southern Spain. Int. J. Geogr. Inf. Sci. 28, 1336–1354.
Rodriguez-Galiano, V., Sanchez-Castillo, M., Chica-Olmo, M., Chica-Rivas, M., 2015. Machine learning predictive models for mineral prospectivity: an evaluation of neural networks, random forest, regression trees and support vector machines. Ore Geol. Rev. 71, 804–818.
Sinclair, A.J., Woodsworth, G.L., 1970. Multiple regression as a method of estimating exploration potential in an area near Terrace, B.C. Econ. Geol. 65, 998–1003.
Singer, D.A., Kouda, R., 1996. Application of a feedforward neural network in the search for Kuroko deposits in the Hokuroku district, Japan. Math. Geol. 28, 1017–1023.
So, C., Zhang, D., Yun, S., Li, D., 1998. Alteration-mineralization zoning and fluid inclusions of the high sulfidation epithermal Cu–Au mineralization at Zijinshan, Fujian Province, China. Econ. Geol. 93, 961–980.
Swets, J.A., Monahan, J., 2000. Psychological science can improve diagnostic decisions. Psychological Science in the Public Interest 1, 1–26.
Wang, S., Pei, R., Zeng, X., Qiu, X., Wei, M., 2009. Metallogenic series and model of the Zijinshan mining field. Acta Geol. Sin. 83, 145–157 (in Chinese with English abstract).
Xia, S., Shen, Y., Zhao, D., Qiu, X., 2015. Lateral variation of crustal structure and composition in the Cathaysia block of South China and its geodynamic implications. J. Asian Earth Sci. 109, 20–28.
Xie, X., Mu, X., Ren, T., 1997. Geochemical mapping in China. J. Geochem. Explor. 60, 99–113.
Xue, K., Ruan, S.K., 2008. Geological characteristics and genesis of the Luobuling copper (molybdenum) deposit in Zijinshan ore-field, Fujian. Resources Environment and Engineering 22, 491–496.
Yousefi, M., Carranza, E.J.M., 2015a. Fuzzification of continuous-value spatial evidence for mineral prospectivity mapping. Comput. Geosci. 74, 97–109.
Yousefi, M., Carranza, E.J.M., 2015b. Prediction–area (P–A) plot and C–A fractal analysis to classify and evaluate evidential maps for mineral prospectivity modeling. Comput. Geosci. 79, 69–81.
Yousefi, M., Carranza, E.J.M., 2015c. Data-driven index overlay and Boolean logic mineral prospectivity modeling in Greenfields exploration. Nat. Resour. Res. http://dx.doi.org/10.1007/s11053-014-9261-9.
Zhang, D., Li, D., Feng, C., Dong, Y., 2001. The temporal and spatial framework of the Mesozoic magmatic system in Zijinshan area and its geological significance. Acta Geosci. Sin. 22, 403–408 (in Chinese with English abstract).
Zhang, D., Feng, C., Li, D., She, H., Dong, Y., 2005. The evolution of ore-forming fluids in the porphyry-epithermal metallogenic system of Zijinshan area. Acta Geosci. Sin. 26, 127–136 (in Chinese with English abstract).
Zhang, Z., Zuo, R., Xiong, Y., 2015. A comparative study of fuzzy weights of evidence and random forests for mapping mineral prospectivity for skarn-type Fe deposits in the southwestern Fujian metallogenic belt, China. Sci. China Earth Sci. http://dx.doi.org/10.1007/s11430-015-5178-3.
Zhao, X., Mao, J., Chen, R., Xu, N., Zeng, Q., Ye, H., 2007. Zircon SHRIMP age and geochemical characteristics of the Caixi pluton in southwestern Fujian Province. Acta Petrol. Mineral. 26, 223–231 (in Chinese with English abstract).
Zhao, X., Mao, J., Chen, R., Xu, N., 2008. SHRIMP zircon dating of the Zijinshan pluton in southwestern Fujian and its implications. Geol. China 35, 590–597 (in Chinese with English abstract).
Zhong, J., Chen, Y., Chen, J., Li, J., Qi, J., Dai, M., 2011. Fluid inclusion study of the Luoboling porphyry Cu–Mo deposit in the Zijinshan ore field, Fujian Province. Acta Petrol. Sin. 27, 1410–1424 (in Chinese with English abstract).
Zhong, J., Chen, Y., Pirajno, F., Chen, J., Li, J., Qi, J., Li, N., 2014. Geology, geochronology, fluid inclusion and H–O isotope geochemistry of the Luoboling Porphyry Cu–Mo deposit, Zijinshan Orefield, Fujian Province, China. Ore Geol. Rev. 57, 61–77.
Zuo, R., 2011. Identifying geochemical anomalies associated with Cu and Pb–Zn skarn mineralization using principal component analysis and spectrum-area fractal modeling in the Gangdese Belt, Tibet (China). J. Geochem. Explor. 111, 13–22.
Zuo, R., 2014. Identification of geochemical anomalies associated with mineralization in the Fanshan district, Fujian, China. J. Geochem. Explor. 139, 170–176.
Zuo, R., Carranza, E.M.J., 2011. Support vector machine: a tool for mapping mineral prospectivity. Comput. Geosci. 37, 1967–1975.
Zuo, R., Wang, J., 2015. Fractal/multifractal modeling of geochemical data: A review. J. Geochem. Explor. http://dx.doi.org/10.1016/j.gexplo.2015.04.010.
Zuo, R., Xia, Q., Zhang, D., 2013. A comparison study of the C–A and S–A models with singularity analysis to identify geochemical anomalies in covered areas. Appl. Geochem. 33, 165–172.